Research Article | Vol. 30, No. 6 / 14 Mar 2022 / Optics Express 8652
Optics EXPRESS

Realistic model of entanglement-enhanced sensing in optical fibers

GREGORY KRUEPER,[1] CHARLES YU,[2] STEPHEN B. LIBBY,[2] ROBERT MELLORS,[2,3] LIOR COHEN,[4] AND JULIET T. GOPINATH[1,4,*]

[1]Department of Physics, University of Colorado Boulder, Boulder, CO 80309, USA
[2]Lawrence Livermore National Laboratory, Livermore, CA 94550, USA
[3]University of California, San Diego, La Jolla, CA 92093, USA
[4]Department of Electrical, Computer and Energy Engineering, University of Colorado Boulder, Boulder, CO 80309, USA
*julietg@colorado.edu

Abstract: Experimental limitations such as optical loss and noise have prevented entanglement-enhanced measurements from demonstrating a significant quantum advantage in sensitivity. Holland-Burnett entangled states can mitigate these limitations and still present a quantum advantage in sensitivity. Here we model a fiber-based Mach-Zehnder interferometer with internal loss, detector efficiency, and external phase noise and without pure entanglement. This model features a practical fiber source that transforms the two-mode squeezed vacuum (TMSV) into Holland-Burnett entangled states. We predict that a phase sensitivity 28% beyond the shot noise limit is feasible with current technology. Simultaneously, a TMSV source can provide about 25 times more photon flux than other entangled sources. This system will make fiber-based quantum-enhanced sensing accessible and practical for remote sensing and probing photosensitive materials.

1. Introduction

Quantum states of light give access to greater sensitivity in measurement than what is possible classically. Shot noise limits classical measurements, in which sensitivity scales as $\bar{n}^{-1/2}$ with an average number of photons $\bar{n}$. With entangled states of light, it is possible to reach the Heisenberg limit, which scales as $\bar{n}^{-1}$, yielding a $\sqrt{\bar{n}}$ enhancement. However, practical implementations remain elusive, due to obstacles such as optical losses, detection efficiency, and the fidelity of the input state.

Some experiments have implemented free-space quantum-enhanced interferometers. At high light levels, a displaced squeezed state can deterministically give a quantum enhancement [1]. However, here we focus on methods using entangled photons, which can demonstrate a higher phase sensitivity *per photon*. Entangled photons have been used to better sense a photosensitive protein [2,3], probe an atomic spin ensemble [4], a nitrogen vacancy center in diamond [5], as well as image a photosensitive birefringent sample [6]. Additionally, fiber-based quantum interferometers may offer simplifications in the phase stabilization of quantum networks [7].

A challenge with many of the experiments is the operation with post-selection, which means that lost photons and incorrect input states are neglected. Including lossy measurements often reduces or eliminates any quantum advantage in sensitivity. One exception is [8], which was performed in free space with two-photon, polarization-entangled N00N states. They limit the need for postselection by reducing the probability of multi-pair generation, at the cost of photon flux. The average photon number per measurement interval $\bar{n}$ was about 0.003 for that experiment. Therefore, future modeling and experiments should focus on refining these techniques with higher photon flux, deterministic input states, and loss tolerance.

#451058 https://doi.org/10.1364/OE.451058
Journal © 2022 Received 12 Dec 2021; revised 14 Jan 2022; accepted 14 Jan 2022; published 1 Mar 2022

Optics EXPRESS

In this work, we model a practical entanglement-enhanced Mach-Zehnder Interferometer (MZI) in optical fiber, including all significant experimental effects and without postselection. We predict that our technique offers a compromise between quantum-enhanced phase sensitivity and overall photon flux; this creates a practical, deterministic, and accessible sensing scheme for photon-starved applications. This model takes losses and external noise that were previously modeled separately [9–13], and cohesively integrates them into a single deterministic framework. In addition, we introduce a new method for handling a finite Hong-Ou-Mandel visibility. The fiber-based design makes the technique accessible for remote sensing applications due to its low loss and flexibility. For two, four, and six-photon entangled states, we demonstrate a quantum advantage in phase sensitivity of 14%, 26%, and 28%, respectively, under experimentally realistic conditions. We also consider a superposition of entangled states obtained from a two-mode squeezed vacuum (TMSV) state, showing a quantum advantage in sensitivity of 28% with the added benefit of roughly 25 times the photon flux as compared to a typical entangled photon source.

Many have modeled quantum-enhanced interferometry with various quantum states of light, each with their own merits and pitfalls [11,14–17]. J. Dowling [15] has pioneered the use of maximally entangled N00N states, which are theoretically optimal, but are especially sensitive to losses [11], and difficult to generate beyond $N = 2$. Alternatively, Holland-Burnett states $HB(N)$ [16] are directly generated by taking N photon pairs from spontaneous parametric downconversion (SPDC) through Hong-Ou-Mandel interference at a beamsplitter. This forms a path-entangled state of the form:

$$\psi = \sum_{i=0}^{N} c_i |2N - 2i, 2i\rangle. \tag{1}$$

While $HB(N)$ accumulate less phase information than N00N states in a lossless interferometer, $HB(N)$ states are more resilient to loss and noise [9].

Others have modeled and demonstrated ways to mitigate the effects of optical loss, noise, and other effects [9,12,13,18–21]. An OAM-enhanced angular displacement estimation scheme was demonstrated to be robust against dark counts and response-time delay [18,19]. By engineering the spatial structure of input photons, it is possible to counteract spectral distinguishability and recover super-sensitivity [20]. Quantum state engineering may also eliminate components of the entangled state that do not accumulate phase information. Examples include the use of non-50:50 beamsplitters [22,23] (at the cost of a lower degree of entanglement) or asymmetric heralded Holland-Burnett states [21].

There is a substantial difference in average photon number between classical interferometry and entanglement-enhanced interferometry. A classical measurement may have 10^{16} photons/s to probe a sample, while a typical entangled photon measurement might have 10^6 photons/s. Due to this large difference in flux, classical measurements will often remain more sensitive. However, for photon-starved applications, where a sample may be destroyed from too much incident power, the sensitivity per photon becomes the figure of merit. This is the regime where quantum metrology is applicable.

2. Methods

2.1. Model setup

Figure 1 illustrates a proposed schematic of our model interferometer. The source of entangled photons is spontaneous parametric downconversion in a waveguide with a $\chi^{(2)}$ nonlinearity. This waveguide converts pump photons into photon pairs via type-II SPDC, which are spatially separated at a polarizing splitter. Rotating one polarization results in indistinguishable photons prior to the first directional coupler, which subsequently produces the entangled Holland-Burnett state $HB(N)$. This first directional coupler begins the MZI, with a bottom sensing branch, and a

Optics EXPRESS

top reference branch. The feedback element $\theta_{feedback}$ ensures that the two parts of the entangled state are matched in path length, allowing for an optimal measurement. The single photon detectors provide photon-number-resolved detection statistics, from which we extract phase information.

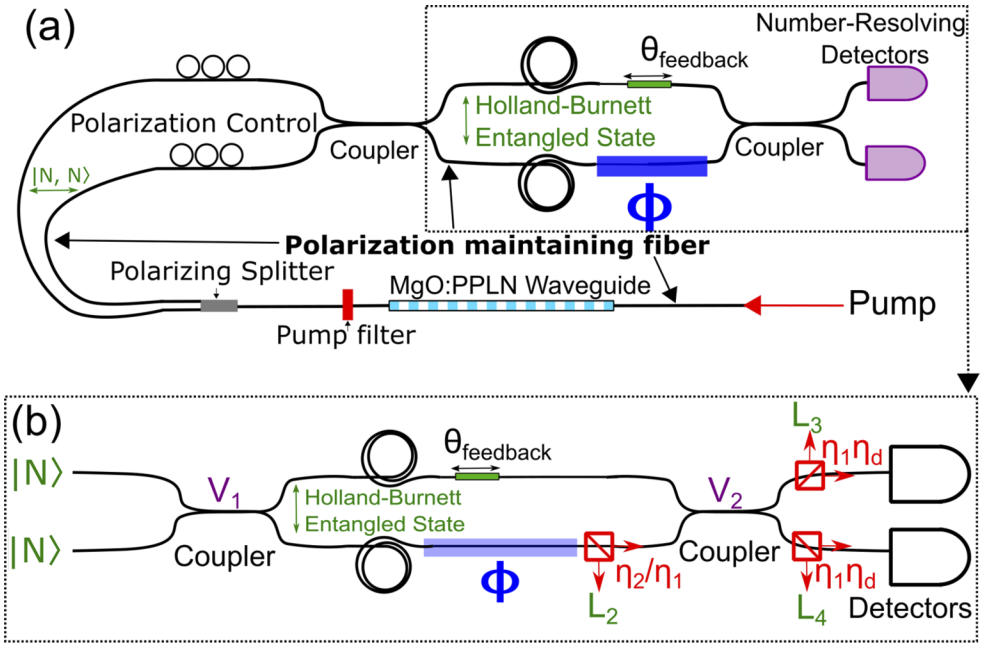

Fig. 1. (a) Schematic of an entanglement-enhanced Mach-Zehnder Interferometer, with equal photon number inputs $|n\rangle$ in each port creating a Holland-Burnett state inside the interferometer. The bottom branch accumulates an unknown phase ϕ while the top branch includes a controllable element $\theta_{feedback}$ that can ensure an optimal measurement. (b) Simplified schematic for modeling. The state experiences loss (red) both inside the interferometer (η_1 and η_2) and in the number-resolving detectors (η_d). The internal loss mode L_1 with loss $1-\eta_1$ is grouped into other losses for simplified analysis.

Other detection options such as homodyne or heterodyne are certainly possible. However, these are capable of phase sensing with a single mode, and so the structure of the Mach-Zehnder interferometer becomes redundant [24]. In other words, adding an external phase reference with a local oscillator creates a different problem than the one we present, and the two problems are not necessarily comparable [25]. We instead focus on the Mach-Zehnder interferometer and how well it can perform for entanglement-enhanced phase estimation, given no external phase reference. Photon number detection then becomes the natural detection method.

Our analysis is restricted to a single frequency mode. Instead of a multimode model, effects such as spectral and spatial overlap between interfering photons are accounted for in the Hong-Ou-Mandel visibility V. We require matching of the interferometer path lengths in order to maximize photon indistinguishability, which is vital for obtaining a reliable entangled state ($V \approx 1$). Also, the range of phases over which phase estimation applies is less than half of a period, where this period is even shorter for an entangled state [26]. To compensate for the small measurement range, as shown in Fig. 1(a), the feedback element $\theta_{feedback}$ can shift so that $\phi - \theta_{feedback}$ is still within range. In practice, $\theta_{feedback}$ could be a varying strain in a section of fiber, adjusting its path length. However, changes in phase must be slower than the measurement speed (for our model, 100 Hz).

Optics EXPRESS

Experimental imperfections will limit the sensitivity of this quantum-enhanced sensor. Detection efficiency has perhaps been the most detrimental of these factors, but recent technological advances show promise in overcoming this obstacle. Both superconducting transition-edge and nanowire sensors have demonstrated with over 90% detection efficiency [27–29], some with inherent photon-number resolution [30–32]. In particular, interfacing a nanowire detector with an impedance-matching taper currently resolves up to 4 photons [30]. With a higher-impedance taper and lower-noise amplifiers, higher photon numbers may be resolved. Efficiently coupling to these detectors is also a significant challenge, but references [32,33] provide methods to obtain up to 99% coupling efficiency with optical fiber. Other common detector metrics like dark count and timing jitter will also degrade performance. Fortunately, compared to the input photon flux of at least 10^6/s, a typical dark count rate of $<10^3$ /s does not contribute any significant error. Additionally, timing jitter is not an issue since the time between pulses (several ns) is much greater than typical timing jitters (several ps). Based on this technological review, we consider it a realistic goal to have detectors with 90% efficiency and number resolution up to 6 in the near future.

A finite degree of entanglement will impair the input state fidelity, and therefore affect the phase sensitivity. The quality of Hong-Ou-Mandel interference in producing an entangled state depends on both the individual spectral purity and the joint indistinguishability of the interfering photons [34,35]. Experimentally, the visibility can be increased by applying narrow spectral filters to the photon pair source, but at the expense of overall photon flux. Recent development in photon sources have demonstrated very high two-photon indistinguishabilities in a variety of sources [36–40]. We expect that a practical implementation of our model based on a MgO:PPLN source can achieve 95% visibility while maintaining a photon flux of around 10^6 /s [40]. In order to maintain this visibility throughout the interferometer, polarization-maintaining fiber must be used to minimize polarization mode dispersion, which could eliminate quantum interference [41].

2.2. Modeling framework

We take a similar approach to other modeling efforts, accounting for internal transmission η (encompassing losses in fiber, fiber couplers and the splitter) and detector efficiency η_d [9], Hong-Ou-Mandel visibility V [39,42,43], and phase noise $\delta\phi$ [10,44]. Our model assumes a visibility of 95%. Based on measurements of phase noise in classical interferometry, we expect about 2 mrad of phase noise in a laboratory-scale experiment [45–47]. We took additional steps to ensure compatibility between these various approaches when integrating them into one model. In the end, for each Holland-Burnett state, the model produces a probability matrix $\rho'_{ij}(\phi)$, representing the probability of detecting i photons in one detector and j photons in the other. This matrix is constructed from a base probability matrix ρ_{ij} that considers losses. See appendix A for more information and appendix C for an example calculation. This base matrix is modified by a finite Hong-Ou-Mandel visibility and external phase noise, as described below.

2.3. Finite visibility

Although modern photon-pair sources can exhibit 99% photon indistinguishability [36,42], some amount of photon distinguishability will affect the degree of entanglement in the interferometer [39]. Interestingly, as our model accounts for every photon input into the system, distinguishable photons cannot be ignored, and will still trigger the detectors. A first-order approximation to a finite distinguishability is that photons will not always undergo Hong-Ou-Mandel interference, and instead act as independent photons throughout the interferometer. As a further complication, this may happen at either the first or second 50:50 beamsplitter. Improper interference can happen with probability $(1 - V)$ where V is the Hong-Ou-Mandel visibility of a given input state. This would then modify the photon detection probability matrix ρ'_{ij} from the original ρ_{ij} with two

Optics EXPRESS

new probability matrices P_{ij} and P'_{ij}. P_{ij} represents the probability matrix from seeing n photons undergo single-photon interference in the interferometer, as they were considered distinguishable at beamsplitter 1 but indistinguishable at beamsplitter 2. This allows for photon self-interference. Similarly, P'_{ij} represents the case where photon pairs are considered distinguishable at beamsplitter 2, no inter-photon interference occurs; no phase information is gained in this case.

$$\rho'_{ij} = V_1 V_2 \rho_{ij} + V_2(1 - V_1)P_{ij} + (1 - V_2)P'_{ij} \tag{2}$$

Here, V_1 and V_2 represent photon visibilities at the first and second beamsplitters, respectively. V_1 may not be equal to V_2 due to a phase mismatch and possible losses during propagation between the two beamsplitters. Note that the sum of all elements in P_{ij} and P'_{ij} equal 1, and that $V_1V_2 + V_2(1 - V_1) + (1 - V_2) = 1$ so that the final probability matrix ρ'_{ij} accounts for all possible events. See Appendix B for the formulation of the P_{ij} matrices for up to 6 photons.

2.4. Phase noise

A degradation in sensitivity in an entanglement-enhanced interferometer from phase noise is explored in [10]. For small amounts of phase noise, a state may undergo phase evolution from a random phase $\delta\phi$. On average, $\langle\delta\phi\rangle = 0$ and $\langle\delta\phi^2\rangle = \Gamma L$ for a dephasing rate Γ over a length L.

$$e^{in\delta\phi} = 1 + in\langle\delta\phi\rangle - \frac{n^2}{2}\langle\delta\phi^2\rangle + \cdots \approx e^{-n^2\Gamma L} \tag{3}$$

An output state will have exponentially lower phase information than normal when subject to phase noise. In our model, we include phase noise by appending $e^{-n^2\Gamma L}$ to each occurrence of $e^{in\phi}$. Although this destroys the normalization of the state, it is still a useful metric to assess sensitivity to phase noise and understand where the quantum advantage in phase sensitivity will be destroyed.

2.5. Quantum Fisher information and the quantum Cramér-Rao bound

The amount of phase information contained in the output state can be calculated with the Fisher information $F(\phi)$ and the photon detection probabilities ρ'_{ij} [48]:

$$F(\phi) = \sum_{i,j} \frac{1}{\rho'_{ij}} \left(\frac{\partial \rho'_{ij}}{\partial \phi}\right)^2. \tag{4}$$

An optimal quantum measurement will extract the maximum information, or the quantum Fisher information, which is obtained from maximizing the Fisher information:

$$F_{quantum} = Max(F(\phi)). \tag{5}$$

In other words, by choosing an optimal ϕ at which to measure, we find the quantum Fisher information. When the measurement is repeated m times, the optimal phase sensitivity is then the quantum Cramér-Rao bound:

$$\Delta\phi_{quantum} = \frac{1}{\sqrt{mF_{quantum}}}. \tag{6}$$

Due to the entanglement-enhanced phase estimation, $\Delta\phi_{quantum}$ should be lower than the shot noise limit:

$$\Delta\phi_{classical} = \frac{1}{\sqrt{m\bar{n}}}. \tag{7}$$

Optics EXPRESS

Since this model uses Holland-Burnett states $HB(N)$ with N pairs of input photons, the phase sensitivity limit in a lossless system with m measurements is [9]:

$$\Delta\phi_{quantum} = \frac{1}{\sqrt{2N(N+1)m}}. \tag{8}$$

This entire operation was performed in parallel for several values of N under realistic conditions.

2.6. Two-mode squeezed vacuum interferometry

Since this model can handle any input state in the Fock state basis, it can also handle superpositions of Fock states. This includes the two-mode squeezed-vacuum (TMSV) state, which can provide more photon flux than a typical entangled photon source, dependent on the degree of squeezing. It has also been theoretically shown that in a lossless interferometer the TMSV can give a phase uncertainty that we will refer to as the theoretical TMSV limit [49]:

$$\Delta\phi = \frac{1}{\sqrt{\bar{n}^2 + 2\bar{n}}}. \tag{9}$$

This slightly exceeds the Heisenberg limit. It may seem that, comparing Eqs. (8) and (9), that the phase sensitivity of a Holland-Burnett (discrete-variable) state is higher than TMSV (a continuous-variable state). Note, however, that a comparison between average photon number and phase sensitivity between discrete and continuous-variable states can be misleading [24]. To avoid confusion, using the TMSV and its average photon number is a fairer, more practical assessment of sensor performance. Also, since the TMSV is the direct output of type-II spontaneous parametric downconversion, it does not need any postselection. This results in more overall photon flux available for the sensor. Therefore, using the TMSV will be highly beneficial to the speed and sensitivity of the sensor in comparison to using individual Holland-Burnett states.

The TMSV state can be described in the photon-number basis as a probability distribution of N pairs of photons [50]:

$$P_N = \frac{(\tanh r)^{2N}}{(\cosh r)^2}, \bar{n} = 2(\sinh r)^2, \tag{10}$$

where r is the squeezing parameter, proportional to the pump power. The two modes in question are usually orthogonal polarizations, but a polarizing beamsplitter can separate these into separate paths as required for this path-entangled interferometer. The entangled state in the interferometer will then be a weighted sum of Holland-Burnett states $HB(N)$:

$$|\psi\rangle = P_0|0,0\rangle + P_1 HB(1) + P_2 HB(2) + \cdots \tag{11}$$

Equation (11) demonstrates the quantum advantage of TMSV with its decomposition into Fock space. Each individual Holland-Burnett state $HB(N)$ has its own quantum advantage (Eq. (8)), and the TMSV gives access to many of these $HB(N)$ states simultaneously, without the need to isolate them with postselection.

The primary limitation on using the two-mode squeezed vacuum comes from the use of photon-number resolving detectors. Since we have assumed a limited number resolution of 6, any part of the squeezed light containing 7 or more photons at one detector must be discarded. For example, an 8-photon event at one detector would suggest a different measured phase than a 10-photon event, but the inability to distinguish these events from each other provides no clear phase estimate. Also, to simplify analysis, we have neglected effects of finite visibility and phase noise in analyzing the TMSV state.

A consequence of limited number resolution is that the squeezing parameter r in our state should not be too high; too much squeezing will contain too many irresolvable, high-photon-number states. With too little squeezing, the sensor will not benefit from the higher entangled states. For a given system efficiency, we have optimized r to produce the most phase information per photon. That is, we choose r such that $F_{quantum}/\bar{n}$ is maximized.

Optics EXPRESS

3. Results

Figure 2 shows the resulting quantum Cramér-Rao bounds from a 2, 4, and 6-photon Holland-Burnett state in the interferometer, as a function of system efficiency $\eta_{sys} = \eta\eta_d$, with our assumed realistic conditions of 95% visibility [43] and 2 mrad of phase noise [47]. To better represent the sensor performance under practical circumstances, we have included an integration time of 10 ms, allowing measurements to be repeated m times, where m is the number of occurrences of that state in 10 ms. We have found this time to be sufficient to accumulate enough photon detection statistics and saturate the sensitivity limit. For Fig. 2, we have assumed an equal flux of each state of 8×10^6 /s. Strictly speaking, if using these states individually, the 4- and 6-photon states would be much less common than the 2-photon state, but for the sake of comparison all fluxes are identical here. Also, for comparison, the equivalent shot noise $1/\sqrt{\eta\eta_d n}$ for each state is also plotted. The intersection of the quantum phase uncertainty for each state with its equivalent shot noise is a good indication for how robust the state is against loss. At 90% internal transmission, the model shows a quantum advantage of 18%, 26%, and 28% beyond the shot noise limit for the 2, 4, and 6-photon states, respectively. These states do no better than shot noise at 59%, 63%, and 65% system efficiency, showing that higher-photon-number states are more sensitive to loss.

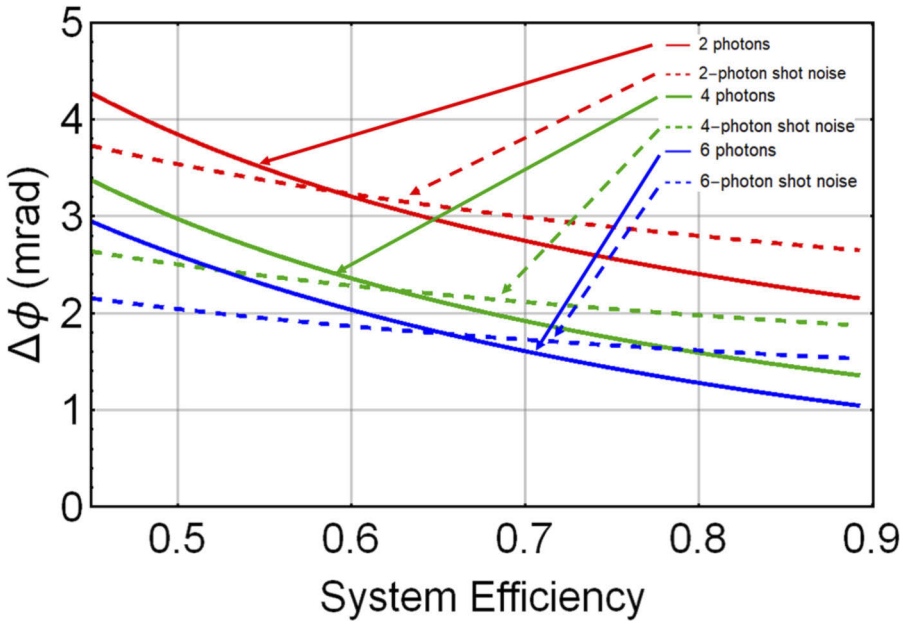

Fig. 2. Phase sensitivity of 2, 4, and 6-photon Holland-Burnett states as a function of system efficiency $\eta_{sys} = \eta\eta_d$. We assume 95% Hong-Ou-Mandel visibility, and 2 mrad of phase noise. Each state's equivalent shot noise $1/\sqrt{\eta\eta_d n}$, is also plotted for comparison. Each state has equal flux, assumed to be 8×10^6 / s, where 10 ms is the sensor integration time.

While Fig. 2 shows a detailed analysis of the lowest three Holland-Burnett states, even higher states are possible in a bright TMSV state. As mentioned earlier, the number of useful states is limited by the two detectors having an assumed number resolution of 6. Fortunately, at an optimal phase and at $\eta_{sys} \approx 81\%$, the most probable outcomes of the 8, 10, 12, and (to an extent) 14-photon Holland-Burnett states are still resolvable. So, despite having more photons than a single detector can resolve, these states still provide significant phase information. From Eq. (11), the TMSV state provides a practical way to access these higher-photon-number states.

Optics EXPRESS

Figure 3 visualizes the Fisher information obtained from each detection event (n_a photons in one branch and n_b photons in the other) for each simulated Holland-Burnett state. These values are weighted by the likelihood of detecting the event. Here, $\eta_{sys} = 81\%$ and $\theta_{feedback}$ is optimal for that state. Despite some detection events exceeding the number resolution of the detectors (n>6, indicated in red), we observe that these events contribute relatively little to the total Fisher information. Instead, the most information is obtained for events where $n_a \approx n_b$. It is not until the 14-photon entangled state that we see significant loss of information from limited number resolution in detectors.

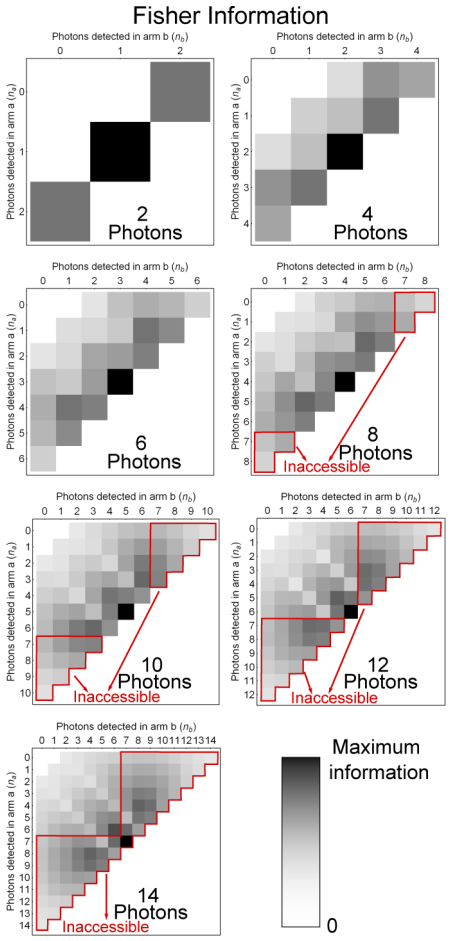

Fig. 3. Matrix plots for the performance of Holland-Burnett states with up to 14 photons when put through the interferometer under realistic conditions and an optimal measurement. The plotted Fisher information for each detection event shows which events give the most phase information. These values are weighted by the likelihood of detecting the event. The red barriers (n>6) correspond to events that the detectors cannot resolve due to limited photon number resolution. The maximum information per event for each plot is scaled differently. For each plot, in order of increasing photon number, the maximum information is 0.93, 2.1, 2.7, 3.9, 4.2, 4.1, and 3.7.

In other words, if N photons are sent through the interferometer, a photon number resolution between $N/2$ and N is sufficient to extract most of the possible phase information. This is due to the fact that an optimal measurement will tend to distribute the photons evenly between the two

Optics EXPRESS

detectors. The exact number resolution that will be sufficient will depend on losses. Overall, this significantly relaxes the photon number resolution requirements on the detectors and shows another advantage to using Holland-Burnett states.

From the discussion following Eq. (11), when using the TMSV in the interferometer, there are competing effects that determine what squeezing parameter r is optimal. Results of this optimization are shown in Fig. 4. In a 100% efficient system, $r_{optimal} = 0.903$, and the corresponding photon number per mode $\bar{n} = 2.13$. We compare this to a typical entangled photon pair source, which intentionally limits $\bar{n}$ to 0.02 [39,40]. The limited $\bar{n}$ ensures that, if any photons are produced, the likelihood of a single pair of photons (99%) is much higher than any other outcome. $\bar{n}$ is proportional to the photon flux of the entangled photon source, and so the increase in $\bar{n}$ for the TMSV source shows up to 107 times the photon flux of a typical entangled source. Near 81% system efficiency, the optimization changes so that we get 25 times the photon flux. This higher photon flux enables faster phase measurements, making the sensor much more practical to use.

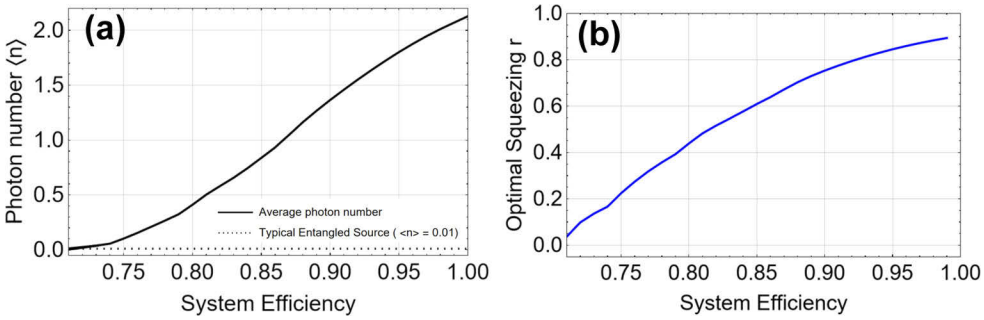

Fig. 4. Results from optimizing a two-mode squeezed vacuum (TMSV) state's squeezing parameter to provide maximum phase information per photon, as a function of system efficiency. We show both (a), the average photon number $\bar{n}$, and (b) the corresponding optimal squeezing parameter r. For comparison, the state's photon number per temporal mode can be compared to that of a typical entangled source $\bar{n} \approx 0.02$. The optimized TMSV can provide 25 times the flux at 80% system efficiency, or 107 times the flux at 100% efficiency.

The other notable feature in Fig. 4 is that $r_{optimal}$ drops to 0 near 70% system efficiency. As seen earlier in Fig. 2, as system efficiency decreases, higher photon-number entangled states tend to lose their quantum advantage earlier than the two-photon state. This means that beyond certain thresholds it is no longer advantageous for an optimized TMSV state to include these states. Consequently, $r_{optimal}$ decreases as efficiency decreases. Taking this to the limit, near 70% efficiency, only the 2-photon entangled state shows a quantum advantage, and so the optimization suppresses any likelihood of seeing higher states. With even lower efficiencies, it will not be practical to use the TMSV state in this manner.

The performance in phase sensitivity of the TMSV state in the interferometer is summarized in Fig. 5. We assume an integration time of 10 ms to represent practical performance. By increasing both photon flux and phase information per photon, the phase sensitivity from the TMSV state scales exponentially with increasing system efficiency. When compared to shot noise, we notice two limits. Near 100% efficiency, we see a 78% sensitivity enhancement. In contrast, near 70% efficiency, this enhancement is only 20%, which marks the point where the quantum advantage of the two-photon state exceeds that of all other states. Thus, the optimization lowers r to below 10^{-3} below 70% efficiency in order to exclusively produce the two-photon state. Under an experimentally achievable 81% system efficiency, the TMSV can provide 25

Optics EXPRESS

times more flux over typical entangled-photon sources [37], and a 28% enhancement in phase sensitivity over shot noise.

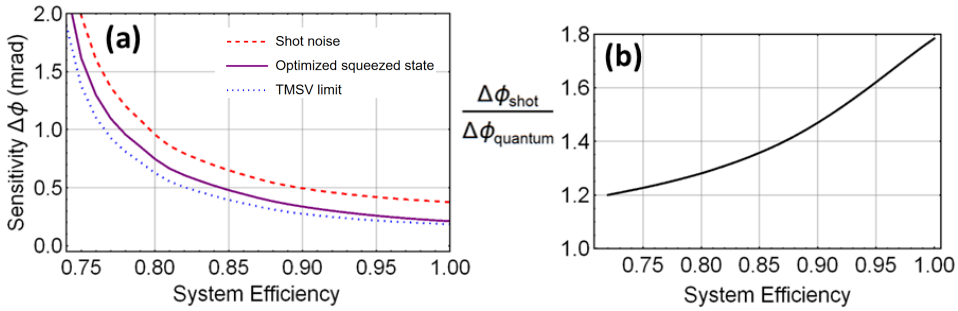

Fig. 5. (a) Phase sensitivity of the optimized TMSV state as a function of system efficiency, given an integration time of 10 ms. For comparison, the equivalent shot noise and the theoretical TMSV limit are plotted as well. (b), The ratio of shot noise and phase sensitivity, showing a quantum advantage varying from 20% to 78% with increasing system efficiency. At 81% system efficiency, the TMSV state provides a 28% phase sensitivity enhancement over shot noise.

These results are consistent with previous models of TMSV phase estimation [49]. When accounting for system losses in the theoretical TMSV limit (Eq. (9)), this method of sensing comes within 14% of the limit near 100% efficiency. We attribute this to the fact that different entangled states have a different optimal phase at which measurement is optimal (Fisher information is maximized). As a combination of all of these states, the TMSV would require $\theta_{feedback}$ to be set to multiple values simultaneously, which is not possible. Instead, the best $\theta_{feedback}$ was chosen as a function of system efficiency, which favored some entangled states over others.

4. Conclusion

Recent advances in quantum optical technology allow for fiber-based entanglement-enhanced interferometry to show a quantum advantage, without post-selection, under realistic conditions. We present a model of a quantum-enhanced fiber interferometer that compromises between phase sensitivity and photon flux to make a practical and accessible sensing scheme. Our modeling results show that, under 90% internal transmission, 90% detection efficiency, 2 mrad of phase noise, and 95% visibility, 2, 4, and 6-photon Holland-Burnett states show a 18%, 26%, and 28% sensitivity improvement beyond the shot-noise limit, on a per-photon basis. When superimposed into a two-mode squeezed vacuum state, these states show a 28% sensitivity improvement while also allowing for 25 times the photon flux of typical entangled-photon sources, which allows for faster measurements. We also show that this sensor may effectively use higher photon-number states than the photon number resolution of a detector would allow. Further improvements in performance can by obtained with improved number-resolving detectors so that the sensor may make use of higher photon-number states. This method may be useful for any photon-starved application, such as probing photosensitive or atomic samples, or transferring information between quantum systems, It may also aid in the phase stabilization of quantum networks. More generally, this model demonstrates a practical, scalable, and robust approach to obtain quantum-enhanced phase information at the few-photon level.

Appendix A

Modeling the interferometer was performed using symbolic math in Wolfram Mathematica, in the photon number basis. By expressing an arbitrary input state in terms of photon creation operators,

Optics EXPRESS

the state can be transformed as an algebraic expression, and represented as a polynomial in creation operators. An input state $|n_a, m_b\rangle$, representing n photons into port a, and m photons into port b, is transformed itno photon creation operators:

$$|\psi_{in}(n,m)\rangle = \frac{1}{\sqrt{n!m!}}(\hat{a^\dagger})^n(\hat{b^\dagger})^m|0\rangle \tag{12}$$

Each operator then transforms as the state propagates through the interferometer. When a state hits a beamsplitter (directional coupler) of coupling ratio t, the operators transform as:

$$\hat{a^\dagger} \rightarrow \sqrt{t}\hat{a^\dagger} + \sqrt{1-t}\hat{b^\dagger} \tag{13}$$

$$\hat{b^\dagger} \rightarrow -\sqrt{1-t}\hat{a^\dagger} + \sqrt{t}\hat{b^\dagger} \tag{14}$$

For instance, a $|1,1\rangle$ state will transform at a 50:50 beamsplitter into $\frac{1}{\sqrt{2}}(|2,0\rangle + |0,2\rangle)$. This implements Hong-Ou-Mandel interference for perfectly indistinguishable photons and creates a path-entangled state. More generally, with N photon pairs, this creates the Holland-Burnett state HB(N).

As $\hat{b^\dagger}$ represents a photon in the sensing arm inside the interferometer, each $\hat{b^\dagger}$ will pick up a phase ϕ as:

$$(\hat{b^\dagger})^n \rightarrow e^{in\phi}(\hat{b^\dagger})^n \tag{15}$$

In this way, the Fock state $|n\rangle$ undergoes phase evolution n times faster than a coherent state. This enhanced phase evolution in Fock states is the basis for achieving super-resolution with entangled photons. Furthermore, to account for loss inside the interferometer η, operators undergo additional splitting into loss modes $\hat{L_1^\dagger}, \hat{L_2^\dagger}$, which are not measured.

$$\hat{a^\dagger} \rightarrow \sqrt{\eta_1}\hat{a^\dagger} + \sqrt{1-\eta_1}\hat{L_1^\dagger} \tag{16}$$

$$\hat{b^\dagger} \rightarrow \sqrt{\eta_2}\hat{b^\dagger} + \sqrt{1-\eta_2}\hat{L_2^\dagger} \tag{17}$$

Here, $\eta_{1,2}$ is the internal transmission of the interferometer in branches a and b. Separate vacuum modes are necessary for each branch to avoid terms with $\hat{L_1^\dagger}$ from cancelling with terms with $\hat{L_2^\dagger}$. Cancellation here would represent photon interference, which is not physical for photons lost in separate branches. Since $[\hat{a^\dagger}, \hat{L_i^\dagger}] = [\hat{b^\dagger}, \hat{L_i^\dagger}] = 0$ for any i, the order in which the phase shift and losses occur does not matter. Thus, this model of one discrete loss is equivalent to a continuous lossy process such as propagation in fiber.

After internal losses, the state is re-combined again at another 50:50 beamsplitter, with the same transformations, allowing for interference effects to become visible. Finite detector efficiency is accounted with additional losses η_d, this time with loss modes $\hat{L_3^\dagger}, \hat{L_4^\dagger}$. However, due to the unitary nature of a beamsplitter, one vacuum mode can be eliminated. Referring to Fig. 1(b), when the reference branch transmission η_1 is higher than the sensing branch transmission η_2, the internal losses can be re-formulated as a common-mode loss η and extra loss in one branch η_2. Then losses can be equivalently formulated by applying loss η_2/η to branch b and losses $\eta\eta_d$ at both detectors. This eliminates the need to include vacuum mode $\hat{L_1^\dagger}$, simplifying the computation for detection probabilities. The red fictional beamsplitters in Fig. 1(b) illustrate this reformulation.

A complex polynomial in terms of operators $\hat{a^\dagger}, \hat{b^\dagger}, \hat{L_2^\dagger}, \hat{L_3^\dagger}, \hat{L_4^\dagger}$ represents the output state. This polynomial is transformed back into the Fock state basis $|j_a, k_b, l_{L2}, m_{L3}, n_{L4}\rangle$ and organized into a rank-5 tensor ρ_{jklmn}. Each element in the tensor represents all coefficients for in the expression proportional to $(\hat{a^\dagger})^j, (\hat{b^\dagger})^k, (\hat{L_2^\dagger})^l, (\hat{L_3^\dagger})^m, (\hat{L_4^\dagger})^n$,. For a general Fock state, $\sqrt{n!}|n\rangle = (\hat{a^\dagger})^n|0\rangle$, so

Optics EXPRESS

the conversion factor for each term in the tensor is $\sqrt{(j!)(k!)(l!)(m!)(n!)}$. Additionally, since vacuum modes are not detected, the sensor should not distinguish between vacuum modes. The detection tensor is flattened into:

$$\rho_{jk} = \sum_{l,m,n} |\rho_{jklmn}|^2 \tag{18}$$

ρ_{jk} then represents the probability of detecting j photons in mode a and k photons in mode b, with any combination of other photons lost to any vacuum mode. For an state input $|n, n\rangle$, ρ_{jk} has dimensions $2n + 1, 2n + 1$, and has nonzero elements for $j + k \leq 2n$. In a lossless environment, only the elements $i, 2n - i$ are nonzero, as all 2n photons are always detected. In a lossy case, however, lower elements may still contain useful phase information. The symbolic form of ρ_{jk} for each Holland-Burnett state is available from the author upon request.

Appendix B: matrices for finite visibility

P_{ij} can be formed from the base probabilities of detection in branches a and b from a single input photon. For brevity, we abbreviate these as x, y, z for describing the probability matrices for events where photons are considered distinguishable.

$$P_a = \frac{\eta_d}{4}(\eta_1 + \eta_2 + 2\sqrt{\eta_1\eta_2}\cos\phi) = x \tag{19}$$

$$P_b = \frac{\eta_d}{4}(\eta_1 + \eta_2 - 2\sqrt{\eta_1\eta_2}\cos\phi) = y \tag{20}$$

$$P_{none} = \frac{1}{2}((1 - \eta_1) + (1 - \eta_2) + \eta_d(\eta_1 + \eta_2)) = z \tag{21}$$

$$P_{2,dist} = \begin{pmatrix} z^2 & 2yz & y^2 \\ 2xz & 2xy & 0 \\ x^2 & 0 & 0 \end{pmatrix} \tag{22}$$

$$P_{4,dist} = \begin{pmatrix} z^4 & 4yz^3 & 6y^2z^2 & 4y^3z & y^4 \\ 4xz^3 & 12xyz^2 & 12xy^2z & 4xy^3 & 0 \\ 6x^2z^2 & 12x^2yz & 6x^2y^2 & 0 & 0 \\ 4x^3z & 4x^3y & 0 & 0 & 0 \\ x^4 & 0 & 0 & 0 & 0 \end{pmatrix} \tag{23}$$

$$P_{6,dist} = \begin{pmatrix} z^6 & 6yz^5 & 15y^2z^4 & 20y^3z^3 & 15y^4z^2 & 6y^5z & y^6 \\ 6xz^5 & 30xyz^4 & 60xy^2z^3 & 60xy^3z^2 & 30xy^4z & 6xy^5 & 0 \\ 15x^2z^4 & 60x^2yz^3 & 90x^2y^2z^2 & 60x^2y^3z & 15x^2y^4 & 0 & 0 \\ 20x^3z^3 & 60x^3yz^2 & 60x^3y^2z & 20x^3y^3 & 0 & 0 & 0 \\ 15x^4z^2 & 30x^4yz & 15x^4y^2 & 0 & 0 & 0 & 0 \\ 6x^5z & 6x^5y & 0 & 0 & 0 & 0 & 0 \\ x^6 & 0 & 0 & 0 & 0 & 0 & 0 \end{pmatrix} \tag{24}$$

Similar combinatorics are used to calculate the matrix P'_{ij}, which represents the probabilities for n single photons to be detected after a beamsplitter with no interference. Due to the lack of

Optics EXPRESS

interference, no phase information is obtained from the events this matrix represents. This is merely for completeness such that the total probability matrix ρ'_{ij} sums to 1.

For a single photon, we have the probabilities of detection:

$$\begin{aligned} P_a &= 0.5\eta_d = x' \\ P_b &= 0.5\eta_d = y' \\ P_{none} &= 1 - \eta_d = z' \end{aligned} \tag{25}$$

For each state, then, P'_{ij} is constructed identically to P_{ij} above, except with x', y', z' instead of x, y, z.

Appendix C: example calculation

Here we provide an example calculation of ρ_{ij}, the probability detection matrix for a 2-photon input. We include one loss mode and phase noise, but skip the visibility. To begin, our input state is:

$$\psi = \hat{a^\dagger}\hat{b^\dagger}|0,0\rangle \tag{26}$$

After the first beamsplitter and a phase shift this becomes:

$$\psi = \frac{1}{2}\left(-\hat{a^\dagger}^2 + \hat{b^\dagger}^2 e^{2i\phi}\right)|0,0\rangle \tag{27}$$

Adding in a loss mode L_2 with transmission η_2:

$$\psi = \left(\frac{-1}{2}\hat{a^\dagger}^2 + \frac{1}{2}e^{2i\phi}\hat{L_2^\dagger}^2(1-\eta_2) + \sqrt{1-\eta_2}\sqrt{\eta_2}e^{2i\phi}\hat{b^\dagger}\hat{L_2^\dagger} + \frac{1}{2}\eta_2 e^{2i\phi}\hat{b^\dagger}^2\right)|0,0,0\rangle \tag{28}$$

After the second beamsplitter, this becomes:

$$\begin{aligned} \psi = \Bigg(&\frac{-1}{4}\hat{a^\dagger}^2 - \frac{1}{2}\hat{a^\dagger}\hat{b^\dagger} - \frac{1}{4}\hat{b^\dagger}^2 + \frac{1}{2}e^{i2\phi}\hat{L_2^\dagger}^2(1-\eta_2) - \frac{1}{\sqrt{2}}\sqrt{\eta_2}\sqrt{1-\eta_2}e^{2i\phi}\hat{a^\dagger}\hat{L_2^\dagger} \\ &+\frac{1}{\sqrt{2}}\sqrt{\eta_2}\sqrt{1-\eta_2}e^{2i\phi}\hat{b^\dagger}\hat{L_2^\dagger} + \frac{1}{4}\eta_2 e^{2i\phi}\hat{a^\dagger}^2 + \frac{1}{2}\eta_2 e^{2i\phi}\hat{a^\dagger}\hat{b^\dagger} + \frac{1}{4}\eta_2 e^{2i\phi}\hat{b^\dagger}^2\Bigg)|0,0,0\rangle \end{aligned} \tag{29}$$

Converting this to a tensor of coefficients for each of the three modes a, b, L_2, we have:

$$\rho_{ijk} = \begin{pmatrix} \begin{Bmatrix} 0 \\ 0 \\ \frac{-1}{\sqrt{2}}e^{2i\phi}(\eta_2 - 1) \end{Bmatrix} & \begin{Bmatrix} 0 \\ \frac{1}{\sqrt{2}}e^{2i\phi}\sqrt{\eta_2(1-\eta_2)} \\ 0 \end{Bmatrix} & \begin{Bmatrix} \frac{1}{2\sqrt{2}}(-1+e^{2i\phi}\eta_2) \\ 0 \\ 0 \end{Bmatrix} \\ \begin{Bmatrix} 0 \\ \frac{1}{\sqrt{2}}e^{2i\phi}\sqrt{\eta_2(1-\eta_2)} \\ 0 \end{Bmatrix} & \begin{Bmatrix} \frac{1}{2}(-1-\eta_2 e^{2i\phi}) \\ 0 \\ 0 \end{Bmatrix} & \begin{Bmatrix} 0 \\ 0 \\ 0 \end{Bmatrix} \\ \begin{Bmatrix} \frac{1}{2\sqrt{2}}(-1+\eta_2 e^{2i\phi}) \\ 0 \\ 0 \end{Bmatrix} & \begin{Bmatrix} 0 \\ 0 \\ 0 \end{Bmatrix} & \begin{Bmatrix} 0 \\ 0 \\ 0 \end{Bmatrix} \end{pmatrix} \tag{30}$$

ρ_{ij} then sums over the third dimension in ρ_{ijk} such that we get a 3 x 3 matrix, and takes the absolute value squared of each element.

Optics EXPRESS

Funding. Lawrence Livermore National Laboratory (DE-AC52-07NA27344); Advanced Research Projects Agency - Energy (DE-AR0001152); National Science Foundation (CCF 1838435); University of Colorado Boulder (QUEST seed grant).

Acknowledgments. We acknowledge useful technical discussions with J. Dowling, K. Shalm, and J. Combes. The portion of this work performed at Lawrence Livermore National Laboratory was under the auspices of the U.S. Department of Energy, under Contract DE-AC52-07NA27344. Publication of this paper was funded by the University of Colorado Boulder Libraries Open Access Fund.

Disclosures. The authors declare no conflicts of interest.

Data availability. Data underlying the results presented in this paper are not publicly available at this time but may be obtained from the authors upon reasonable request.

References

1. C. Schäfermeier, M. Ježek, L. S. Madsen, T. Gehring, and U. L. Andersen, "Deterministic phase measurements exhibiting super-sensitivity and super-resolution," Optica **5**(1), 60–64 (2018).
2. A. Crespi, M. Lobino, J. C. F. Matthews, A. Politi, C. R. Neal, R. Ramponi, R. Osellame, and J. L. O'Brien, "Measuring protein concentration with entangled photons," Appl. Phys. Lett. **100**(23), 233704 (2012).
3. J. Haas, M. Schwartz, U. Rengstl, M. Jetter, P. Michler, and B. Mizaikoff, "Chem/bio sensing with non-classical light and integrated photonics," The Analyst **143**(3), 593–605 (2018).
4. F. Wolfgramm, C. Vitelli, F. A. Beduini, N. Godbout, and M. W. Mitchell, "Entanglement-enhanced probing of a delicate material system," Nat. Photonics **7**(1), 28–32 (2013).
5. G.-Q. Liu, Y.-R. Zhang, Y.-C. Chang, J.-D. Yue, H. Fan, and X.-Y. Pan, "Demonstration of entanglement-enhanced phase estimation in solid," Nat. Commun. **6**(1), 6726 (2015).
6. Y. Israel, S. Rosen, and Y. Silberberg, "Supersensitive polarization microscopy using noon states of light," Phys. Rev. Lett. **112**(10), 103604 (2014).
7. S. Yanikgonul, R. Guo, A. Xomalis, A. N. Vetlugin, G. Adamo, C. Soci, and N. I. Zheludev, "Phase stabilization of a coherent fiber network by single-photon counting," Opt. Lett. **45**(10), 2740–2743 (2020).
8. S. Slussarenko, M. M. Weston, H. M. Chrzanowski, L. K. Shalm, V. B. Verma, S. W. Nam, and G. J. Pryde, "Unconditional violation of the shot-noise limit in photonic quantum metrology," Nat. Photonics **11**(11), 700–703 (2017).
9. A. Datta, L. Zhang, N. Thomas-Peter, U. Dorner, B. J. Smith, and I. A. Walmsley, "Quantum metrology with imperfect states and detectors," Phys. Rev. A **83**(6), 063836 (2011).
10. B. Roy Bardhan, K. Jiang, and J. P. Dowling, "Effects of phase fluctuations on phase sensitivity and visibility of path-entangled photon Fock states," Phys. Rev. A **88**(2), 023857 (2013).
11. M. A. Rubin and S. Kaushik, "Loss-induced limits to phase measurement precision with maximally entangled states," Phys. Rev. A **75**(5), 053805 (2007).
12. U. Dorner, R. Demkowicz-Dobrzanski, B. J. Smith, J. S. Lundeen, W. Wasilewski, K. Banaszek, and I. A. Walmsley, "Optimal quantum phase estimation," Phys. Rev. Lett. **102**(4), 040403 (2009).
13. S. D. Huver, C. F. Wildfeuer, and J. P. Dowling, "Entangled fock states for robust quantum optical metrology, imaging, and sensing," Phys. Rev. A **78**(6), 063828 (2008).
14. J. Joo, W. J. Munro, and T. P. Spiller, "Quantum Metrology with Entangled Coherent States," Phys. Rev. Lett. **107**(8), 083601 (2011).
15. J. P. Dowling, "Quantum optical metrology - The lowdown on high-N00N states," Contemp. Phys. **49**(2), 125–143 (2008).
16. R. B. Jin, M. Fujiwara, R. Shimizu, R. J. Collins, G. S. Buller, T. Yamashita, S. Miki, H. Terai, M. Takeoka, and M. Sasaki, "Detection-dependent six-photon Holland-Burnett state interference," Sci. Rep. **6**(1), 36914 (2016).
17. J. Sahota and D. F. V. James, "Quantum-enhanced phase estimation with an amplified Bell state," Phys. Rev. A **88**(6), 063820 (2013).
18. J. Zhang, Z. Zhang, L. Cen, M. Yu, S. Li, F. Wang, and Y. Zhao, "Effects of imperfect elements on resolution and sensitivity of quantum metrology using two-mode squeezed vacuum state," Opt. Express **25**(21), 24907–24916 (2017).
19. J.-D. Zhang, Z.-J. Zhang, L.-Z. Cen, C. You, S. Adhikari, J. P. Dowling, and Y. Zhao, "Orbital-angular-momentum-enhanced estimation of sub-heisenberg-limited angular displacement with two-mode squeezed vacuum and parity detection," Opt. Express **26**(13), 16524–16534 (2018).
20. M. Jachura, R. Chrapkiewicz, R. Demkowicz-Dobrzański, W. Wasilewski, and K. Banaszek, "Mode engineering for realistic quantum-enhanced interferometry," Nat. Commun. **7**(1), 11411 (2016).
21. G. S. Thekkadath, M. E. Mycroft, B. A. Bell, C. G. Wade, A. Eckstein, D. S. Phillips, R. B. Patel, A. Buraczewski, A. E. Lita, T. Gerrits, S. W. Nam, M. Stobińska, A. I. Lvovsky, and I. A. Walmsley, "Quantum-enhanced interferometry with large heralded photon-number states," npj Quantum Inform. **6**(1), 89 (2020).
22. B. H. Liu, F. W. Sun, Y. X. Gong, Y. F. Huang, G. C. Guo, and Z. Y. Ou, "Four-photon interference with asymmetric beam splitters," Opt. Lett. **32**(10), 1320–1322 (2007).
23. M. Kacprowicz, R. Demkowicz-Dobrzański, W. Wasilewski, K. Banaszek, and I. A. Walmsley, "Experimental quantum-enhanced estimation of a lossy phase shift," Nat. Photonics **4**(6), 357–360 (2010).

Optics EXPRESS

24. D. Branford and J. Rubio, "Average number is an insufficient metric for interferometry," New J. Phys. **23**(12), 123041 (2021).
25. M. Jarzyna and R. Demkowicz-Dobrzański, "Quantum interferometry with and without an external phase reference," Phys. Rev. A **85**(1), 011801 (2012).
26. K. Jiang, C. J. Brignac, Y. Weng, M. B. Kim, H. Lee, and J. P. Dowling, "Strategies for choosing path-entangled number states for optimal robust quantum-optical metrology in the presence of loss," Phys. Rev. A **86**(1), 013826 (2012).
27. M. Rajteri, E. Taralli, C. Portesi, E. Monticone, and J. Beyer, "Photon-number discriminating superconducting transition-edge sensors," Metrologia **46**(4), S283–S287 (2009).
28. D. Rosenberg, A. J. Kerman, R. J. Molnar, and E. a. Dauler, "Nanowire Single Photon Detector Array," Opt. Express **21**(2), 1440–1447 (2013).
29. V. B. Verma, B. Korzh, F. Bussières, R. D. Horansky, S. D. Dyer, A. E. Lita, I. Vayshenker, F. Marsili, M. D. Shaw, H. Zbinden, R. P. Mirin, and S. W. Nam, "High-efficiency superconducting nanowire single-photon detectors fabricated from MoSi thin-films," Opt. Express **23**(26), 33792–33801 (2015).
30. D. Zhu, M. Colangelo, C. Chen, B. A. Korzh, F. N. Wong, M. D. Shaw, and K. K. Berggren, "Resolving photon numbers using a superconducting nanowire with impedance-matching taper," Nano Lett. **20**(5), 3858–3863 (2020).
31. M. Jönsson, M. Swillo, S. Gyger, V. Zwiller, and G. Björk, "Temporal array with superconducting nanowire single-photon detectors for photon-number resolution," Phys. Rev. A **102**(5), 052616 (2020).
32. F. Marsili, V. B. Verma, J. A. Stern, S. Harrington, A. E. Lita, T. Gerrits, I. Vayshenker, B. Baek, M. D. Shaw, R. P. Mirin, and S. W. Nam, "Detecting single infrared photons with 93% system efficiency," Nat. Photonics **7**(3), 210–214 (2013).
33. A. J. Miller, A. E. Lita, B. Calkins, I. Vayshenker, S. M. Gruber, and S. W. Nam, "Compact cryogenic self-aligning fiber-to-detector coupling with losses below one percent," Opt. Express **19**(10), 9102–9110 (2011).
34. C. I. Osorio, N. Sangouard, and R. T. Thew, "On the Purity and Indistinguishability of Down-Converted Photons," J. Phys. B: At., Mol. Opt. Phys. **46**(5), 055501 (2013).
35. R. Okamoto, H. F. Hofmann, T. Nagata, J. L. O'Brien, K. Sasaki, and S. Takeuchi, "Beating the standard quantum limit: phase super-sensitivity of N -photon interferometers," New J. Phys. **10**(7), 073033 (2008).
36. H. Wang, H. Hu, T.-H. Chung, J. Qin, X. Yang, J.-P. Li, R.-Z. Liu, H.-S. Zhong, Y.-M. He, X. Ding, Y.-H. Deng, Q. Dai, Y.-H. Huo, S. Höfling, C.-Y. Lu, and J.-W. Pan, "On-Demand Semiconductor Source of Entangled Photons Which Simultaneously Has High Fidelity, Efficiency, and Indistinguishability," Phys. Rev. Lett. **122**(11), 113602 (2019).
37. T. Zhong, F. N. C. Wong, T. D. Roberts, and P. Battle, "High performance photon-pair source based on a fiber-coupled periodically poled KTiOPO4 waveguide," Opt. Express **18**(19), 20114 (2010).
38. F. Zhu, W. Zhang, and Y. Huang, "Fiber-based frequency-degenerate polarization entangled photon pair sources for information encoding," Opt. Express **24**(22), 25619–25628 (2016).
39. A. Villar, A. Lohrmann, and A. Ling, "Experimental entangled photon pair generation using crystals with parallel optical axes," Opt. Express **26**(10), 12396–12402 (2018).
40. J. Zhao, C. Ma, M. Rüsing, and S. Mookherjea, "High Quality Entangled Photon Pair Generation in Periodically Poled Thin-Film Lithium Niobate Waveguides," Phys. Rev. Lett. **124**(16), 163603 (2020).
41. S. P. Walborn, A. N. de Oliveira, S. Pádua, and C. H. Monken, "Multimode Hong-Ou-Mandel Interference," Phys. Rev. Lett. **90**(14), 143601 (2003).
42. E. Roccia, V. Cimini, M. Sbroscia, I. Gianani, L. Ruggiero, L. Mancino, M. G. Genoni, M. A. Ricci, and M. Barbieri, "Multiparameter approach to quantum phase estimation with limited visibility," Optica **5**(10), 1171–1176 (2018).
43. H. Takesue and K. Shimizu, "Effects of multiple pairs on visibility measurements of entangled photons generated by spontaneous parametric processes," Opt. Commun. **283**(2), 276–287 (2010).
44. B. M. Escher, R. L. De Matos Filho, and L. Davidovich, "General framework for estimating the ultimate precision limit in noisy quantum-enhanced metrology," Nat. Phys. **7**(5), 406–411 (2011).
45. J. Minár, H. de Riedmatten, C. Simon, H. Zbinden, and N. Gisin, "Phase-noise measurements in long-fiber interferometers for quantum-repeater applications," Phys. Rev. A **77**(5), 052325 (2008).
46. Y. Pang, J. J. Hamilton, and J.-P. Richard, "Frequency noise induced by fiber perturbations in a fiber-linked stabilized laser," Appl. Opt. **31**(36), 7532–7534 (1992).
47. S. Knudsen, A. B. Tveten, and A. Dandridge, "Measurements of Fundamental Thermal Induced Phase Fluctuations in the Fiber of a Sagnac Interferometer," IEEE Photonics Technol. Lett. **7**(1), 90–92 (1995).
48. S. L. Braunstein and C. M. Caves, "Statistical distance and the geometry of quantum states," Phys. Rev. Lett. **72**(22), 3439–3443 (1994).
49. P. M. Anisimov, G. M. Raterman, A. Chiruvelli, W. N. Plick, S. D. Huver, H. Lee, and J. P. Dowling, "Quantum Metrology with Two-Mode Squeezed Vacuum: Parity Detection Beats the Heisenberg Limit," Phys. Rev. Lett. **104**(10), 103602 (2010).
50. P. Gerry and C. Knight, *Introductory Quantum Optics* (Cambridge, 2004).